42nd AIAA Aerospace Sciences Meeting and Exhibit
5-8 January 2004/Reno, NV

STUDY OF THREE-DIMENSIONAL SYNTHETIC JET FLOWFIELDS USING DIRECT NUMERICAL SIMULATION.

B.R.Ravi* and R. Mittal†,
Department of Mechanical & Aerospace Engineering,
The George Washington University,
Washington DC 20052

F.M. Najjar‡
Center for Simulation of Advanced Rockets
University of Illinois at Urbana-Champaign
Urbana, IL 61801

ABSTRACT

The formation and evolution of 3D synthetic jets is examined using direct numerical simulations. The primary focus of the current study is on examining the formation of 3D synthetic jets and the effect of changes in the jet aspect-ratio on the flow produced by the jet. Jets in quiescent and cross-flow cases are investigated. The study compares the vortex dynamics, velocity profiles and the other dynamical characteristics of the jet for the various cases which allows us to extract some insight into the effect of these modifications on the jet performance. It is expected that the study will lead to a better understanding of the behavior of 3D synthetic jets.

INTRODUCTION

Synthetic jets are being used in a number of flow-control applications ranging from thrust vectoring of jet engines[1,2] mixing enhancement[3,4] to active control of separation and turbulence [5,6,7,8] in boundary layers. A detailed parametric study of 2D (infinite aspect ratio) synthetic jets [9,10,11] has been carried out where the effects of variation in the operational parameters such as diaphragm amplitude and slot dimensions as well as external flow characteristics has been examined. However, since most synthetic jets in practical applications have finite aspect-ratio and therefore have strongly three-dimensional characteristics, a detailed study of 3D synthetic jet flow fields would be quite useful. In the current study, three-dimensional direct numerical simulations are used to investigate fundamental aspects of synthetic jet flow fields.

The eventual goal is to distill our understanding into scaling laws that can be used in the design of such devices and this forms the motivation for the current study.

FLOW CONFIGURATION AND SIMULATION APPROACH

A schematic of a synthetic jet device which can be flush-mounted on the suction surface of an airfoil is shown in figure 1. The synthetic jet consists of a piezoelectric membrane mounted onto a metal diaphragm, which is sealed to form a cavity. The rectangular cavity is defined by width (W), depth (D) and height (H). A slot type is chosen for the jet and is characterized by the width (d), height (h) and depth (w). Fluid is periodically expelled and entrained from and into the cavity by the oscillation of the diaphragm which is characterized by the deflection amplitude (A) and angular frequency (ω). Note that jet actuation may also be accomplished by other means such as an oscillating piston. The external flow is characterized by a freestream velocity (U_∞) and the boundary layer thickness (δ). The fluid is characterized by the kinematic viscosity (ν) and density (ρ). The flow inside the cavity is treated as incompressible assuming that the actual devices will be designed to operate in the same flow regime.

Jet Characterization and Scaling

The exit flow emanating from the slot is a function of both space and time and hence can be characterized by a number of different parameters. In past studies[9,10] we have parameterized the jet though various "moments" of the jet velocity profile where the nth moment of the jet profile is defined as

$$C^n_{\phi 12} = \frac{1}{t_2 - t_1}\int_{t_1}^{t_2}\frac{1}{w}\int_{-w/2}^{w/2}\frac{1}{d}\int_{-d/2}^{d/2}\left[V_j(x,z,t)\right]^n dx dz dt \qquad (1)$$

---

* Student Member AIAA, Graduate Research Assistant
† Senior Member AIAA, Associate Professor
‡ Principal Research Scientist

Here V_j is the jet velocity normalized by a suitable scale (freestream velocity or inviscid jet velocity). It is noted from earlier simulations that the jet exit flow is significantly different during the expulsion and ingestion phases and therefore it is more appropriate to define the moments separately for these phases denoted by C^n_{ex} and C^n_{in} respectively. Such a characterization forms the basis of a systematic framework for the development of scaling laws. Furthermore a number of these moments have a direct physical significance. For instance, $C^1_{ex}+C^1_{in}$ represents the mass flux, which for a synthetic jet is identically zero. Similarly the quantities $C^2_{ex} + C^2_{in}$ and $C^3_{ex} + C^3_{in}$ represent the momentum and the kinetic energy flux of the jet. The functional dependence of these parameters can be written in terms of the key non-dimensional parameters

$$(C^n_{ex}; C^n_{in}) = fn\left(\frac{w}{d}, \frac{h}{L_j}, \frac{\overline{V}_j L_j}{\nu}, \sqrt{\frac{\omega L_j^2}{\nu}}, \frac{U_\infty \delta}{\nu}, \frac{\delta}{d}\right) \quad (2)$$

where

$L_j = (d \times w)^{1/2}$: jet area based length scale

$\overline{V}_j L_j / \nu = Re_J$; jet Reynolds where $\overline{V}_j$ is the average jet velocity

h / L_j: slot height to slot area ratio

w/d: slot aspect-ratio

$\sqrt{\omega L_j^2 / \nu} = S$: Stokes number

$U_\infty \delta / \nu = Re_\delta$: Reynolds number based on boundary layer thickness

δ / d: boundary layer thickness to slot width ratio

The current study focuses on the effect of varying *w/d* retaining all other cavity parameters the same.

Simulation Approach

The current simulations are carried out using a 3D Cartesian, Incompressible, Navier-Stokes solver, VICAR3D, developed recently. The solver allows simulation of unsteady viscous flows with complex immersed boundaries on Cartesian grids. The use of a Cartesian grid simplifies the meshing of the flow domain. The solver employs a second-order accurate central-difference scheme for the spatial discretization and a two-step fractional-step scheme for time advancement.

For the current flow, the key advantage using the solver is that the entire geometry is modeled on a stationary Cartesian mesh. Figure 1 shows a typical schematic of the geometry and Figure 2 shows the mesh used in the simulations. In addition, suitable boundary conditions are to be prescribed for the external flow. For quiescent external flow case, a soft velocity boundary condition is applied on the north, east and west boundaries thereby allowing the conditions at these boundaries to respond freely to the flow created by the jet. For the simulation of jet in a cross-flow, a Blasius boundary layer profile is imposed at the west boundary whereas soft boundary conditions are applied at the north and east boundaries.

SIMULATION RESULTS

Here we describe the vortex dynamics and jet characteristics observed for several cases. Three different jet slot configuration are investigated and for each of these, simulations are carried out with and without external cross-flow. For the current study the h/L_j, δ/d and Re_J are fixed at values of 1.46, 2.0 and 227 respectively. In the cases with external cross-flow the boundary layer Reynolds number is fixed such that $\overline{V}_j / U_\infty$ = 0.5. The slot modification is subject to the constraint that the slot area and average jet exit velocity remains the same.

Slot Configurations

Figure 3 shows schematic of the three different slot configurations examined in the current study. Case 1 consists of a slot with aspect ratio *w/d*=1 (square slot). Case 2 consists of a slot with aspect ratio *w/d*=2 and such that the slot area is same as that in case 1 and the same volume of fluid flows across the slot when the average jet velocity is held fixed. Case 3 consist of a slot with *w/d*=4. The grid size is fixed as 101^3 for the first three cases corresponding to jet in quiescent case. We first compare the performance of the jets with the quiescent external flow. This is followed up by a similar comparison in the situation where there is an external crossflow.

Jet in Quiescent External Flow

Figure 4 shows the iso-surfaces of eigenvalue contours, obtained from deformation matrix, for all the cases and this provides a qualitative view of the effect of the modification of the slot geometry on the vortices produced by the jet. As expected, changes in the slot configuration have a large impact on the corresponding outflow as visible from the significant changes in the vortex structure topology. For all the slot shapes considered in the current study, the average jet exit velocity, $\overline{V}_j$, and the slot area are held fixed. The Stokes numbers are 10.8, 12 and 15.2 respectively corresponding to *w/d*=1, 2 and 4. This was done to keep $Re_J / S^2 > 0.2$ since this parameter has been found to be key in determining jet formation[10]. It is noticed from

figure 4(a), that for the square slot a distinct vortex ring emerges out during the peak expulsion phase. The Figure 4(b) corresponds to the case when the slot is rectangular with aspect ratio equal to 2. It is interesting to note that the rectangular vortex ring that emerges out of this slot rotates in its own plane by 90 degrees as it convects upwards and becomes perpendicular to the slot. This is very similar to the "axis-switching" phenomenon seen for steady jets[12]. Axis switching is even more clearly visible in Figure 4(c) for which *w/d*=4. The corresponding plot at the spanwise midpoint of the slot in the XY-plane is presented in the Figure 5 for all the slot shapes and cases considered. The plots correspond to the maximum expulsion phase for all the cases.

Further insight into the effect of slot modifications can be gained by examining the jet velocity profile at the slot exit. Figure 6 shows these profiles normalized using the average inviscid jet velocity, for the various cases at two different phases of the cycle. It is observed from figure 6(a) that for square slot the velocity profile appears 'jet-like' in the maximum expulsion phase and is more 'plug-like' during the maximum ingestion phase. The normalized velocity is about 2.4 at maximum expulsion and 2.1 at maximum ingestion. Note that the x and z coordinate values are normalized using the slot width (d) and slot depth (w) respectively in order to compare the cases considered here. It is observed from figure 6(b) that for a rectangular slot with *w/d=2,* the jet exit profile tends to become more parabolic. However, there is no significant change in the peak value of the normalized jet exit velocity. It is also clear from figure 6(c) for rectangular slot with *w/d*=4, the jet exit velocity is more parabolic than for *w/d*=2. A similar trend is observed with reference to the jet velocities during ingestion phase as well and is apparent from the figures 6(a) to 6(c). A comparison of velocity profiles is presented in figure 6(d) at slot center for maximum expulsion and maximum ingestion phases.

Jet in External Cross-Flow

In this section we describe the simulation results for the same three slot configurations discussed in the previous section, except that here an external cross-flow is imposed on the jet. The external flow is a Blasius flat-plate boundary layer profile with boundary layer thickness based Reynolds number, Re_δ=906.4, 641.4 and 453.1 corresponding to *w/d*=1,2,4 respectively, such that δ/d=2. For all the cases the ratio $\bar{V}_j / U_\infty$ was held at 0.5. For all the finite aspect-ratio slots, we observe the formation of a sequence of vortex-loop type structures that convect downstream in the boundary layer. Figure 7 shows the iso-surfaces of eigenvalue contours. Notice the clear vortex rings in the streamwise direction at about a cavity length distance from the slot center. The vortex rings formed penetrate the boundary layer and emerge out of the boundary layer indicating that 3D jets have more impulse than their 2D counterpart. This will be confirmed when, later in the paper the jet momentum coefficients are computed. Figure 8 shows spanwise vorticity plots in the XY-plane at the slot center at the maximum expulsion phase. The flow inside the cavity is asymmetric for all the cases due to the imposed external flow. It is observed that in all the cases, a shear layer is formed at the jet exit. The computed velocities at the jet exit (figure 9) also show some differences between various cases considered. A general trend that is observed from all the cases indicates there is a shift of the velocity profiles to the right making it unsymmetrical about the center-line of the slot. It is noticed from figure 9(d) that during the maximum ingestion phase the velocity profiles tends to be more "peaky" as *w/d* increases.

Jet Moment Coefficients

The computed normalized momentum coefficients for both the quiescent jet and the jet in crossflow are presented in figure 10. The momentum coefficient has been normalized by the momentum coefficient of the corresponding inviscid jet. Since the behavior of the jet profile is markedly different during the expulsion and ingestion strokes, the momentum coefficient has been computed and plotted separately for the two phases. Interestingly it is observed that the momentum coefficient during the expulsion phase is lower than in the ingestion phase for all the cases considered even for the quiescent flow. This is attributed to the fact that the velocity exhibits more "plug-like" behavior (figures 4 and 7) during the ingestion phase having a higher absolute value near the slot end walls in comparison with its expulsion counterpart of the velocity at the same x and z stations thus contributing to the extra momentum during the ingestion phase. Overall, the total momentum coefficient is about 1.6 for all the three cases studied here and the simulations indicate that the momentum coefficient is relatively insensitive to the jet aspect ratio.

Figure 10(b) shows the corresponding plot for the jet in crossflow. For this flow configuration also it is observed that the momentum coefficient is relatively insensitive to the slot aspect ratio. The overall momentum coefficient has a value 1.8 which is noticeably higher than the jets in quiescent flow.

CONCLUSIONS

Direct numerical simulations have been used to study the formation and interaction of a synthetic jet with a flat plate boundary layer in a three-dimensional configuration. The motion of the diaphragm is modeled using appropriate boundary conditions at the bottom of the cavity. The simulations show that in presence of crossflow, the evolution of the vortex structures and the velocity profiles differ significantly. Separate analysis of the ingestion and expulsion phases is found to be useful since it reveals a better insight into the jet behavior when there is a crossflow. The solver is being parallelized and this should allow us to access a larger parameter range for these flows.

ACKNOWLEDGEMENTS

This work is supported by NASA Grant NAG-1-01024 and AFOSR Grant F49620-03-1-0146.

REFERENCES

1. Wygnanski, I., (1997), Boundary Layer and Flow Control by Periodic Addition of Momentum, AIAA 97-2117.
2. Amitay, M., Kibens,V., Parekh, D., and Glezer, A., (1999), The Dynamics of Flow Reattachment Over a Thick Airfoil Controlled by Synthetic Jet Actuators, AIAA 99-1001.
3. Chen, Y., Liang, S., Anug, K., Glezer, A., Jagoda, J. (1999), Enhanced mixing in a Simulated Combustor Using Synthetic Jet Actuators. AIAA 99-0449.
4. Davis, S. A., Glezer, A., (1999), Mixing Control of Fuel Jets Using Synthetic Jet Technology : Velocity Field Measurement, AIAA 99-0447.
5. Lee, C.Y., and Goldstein, D.B., (2001), DNS of microjets for Turbulent Boundary Layer Control, AIAA 2001-1013.
6. Amitay, M., Honohan, A., Trautman, M, Glezer, A., (1997), Modification of the Aerodynamic Characteristic of Bluff Bodies Using Fluidic Actuators, AIAA 97-2004.
7. Smith, D., Amitay, M., Kibens, V., Parekh, D., Glezer, A, (1998), Modification of Lifting Body Aerodynamics Using Synthetic Jet Actuators, AIAA 98-0209.
8. Crook, A., Sadri, M., Wood, N. J. (1999), The Development and Implementation of Synthetic Jets for the control of separated flow, AIAA 99- 3176.
9. Mittal, R., Rampunggoon, P., Udaykumar, H.S., Interaction of a Synthetic Jet with a Flat Plate Boundary Layer, (2001), AIAA 2001-2773.
10. Utturkar, Y., Holman, R., Mittal, R., Caroll, R., Sheplak, M., and Cattafesta, L., (2003), A Jet formation Criterion for Synthetic Jet Actuators, AIAA 2003-0636.
11. Rampunggoon, P., Interaction of a Synthetic Jet with a Flat Plate Boundary Layer, (2001), Ph.D Thesis, University of Florida, Gainesville, FL, USA.
12. Wilson, R.W., Demuren, A.O, (1997), Numerical Simulation of turbulent jets with rectangular cross section, NASA CR-201642 ICASE Report No. 97-1.

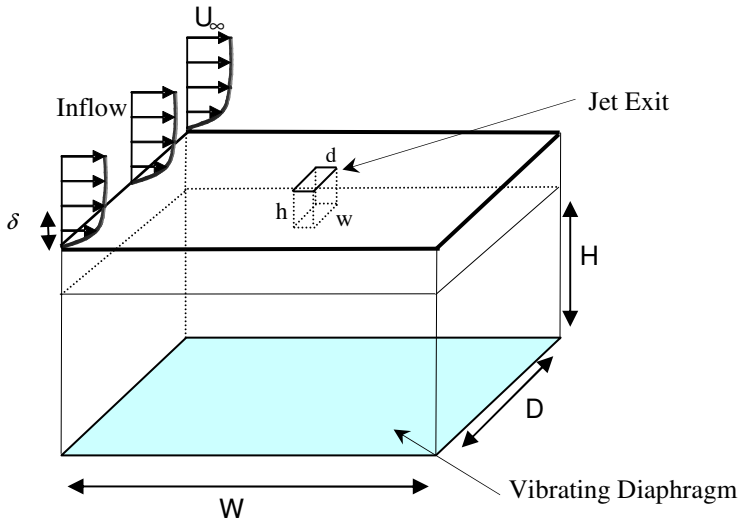

Figure 1 Schematic of a synthetic jet

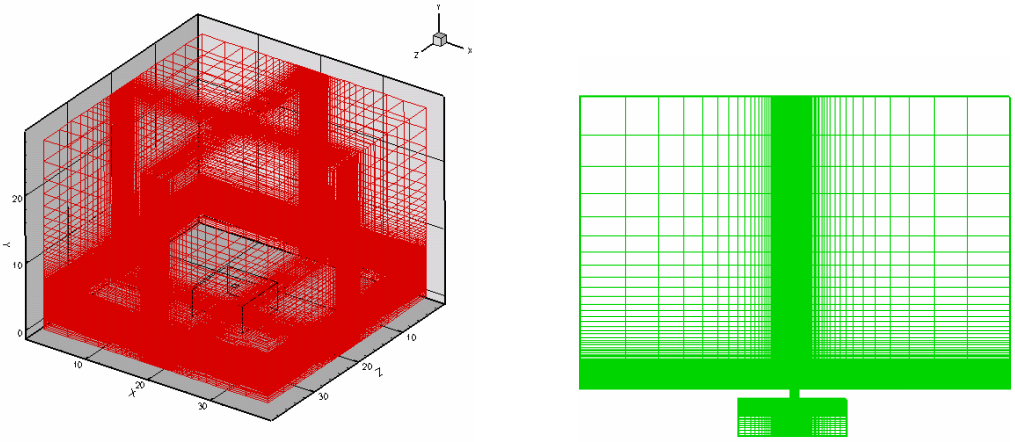

(a) (b)

Figure 2 (a) Typical 3D mesh used in computations showing the cavity
(b) Mesh as viewed the XY-Plane.

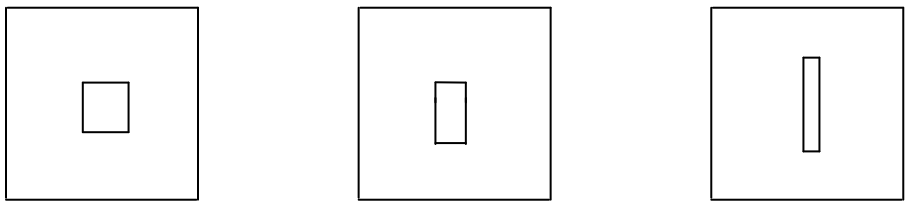

(a) (b) (c)

Figure 3 (a) Square slot (b) Rectangular slot, *w/d = 2* (c) Rectangular slot, *w/d=4*

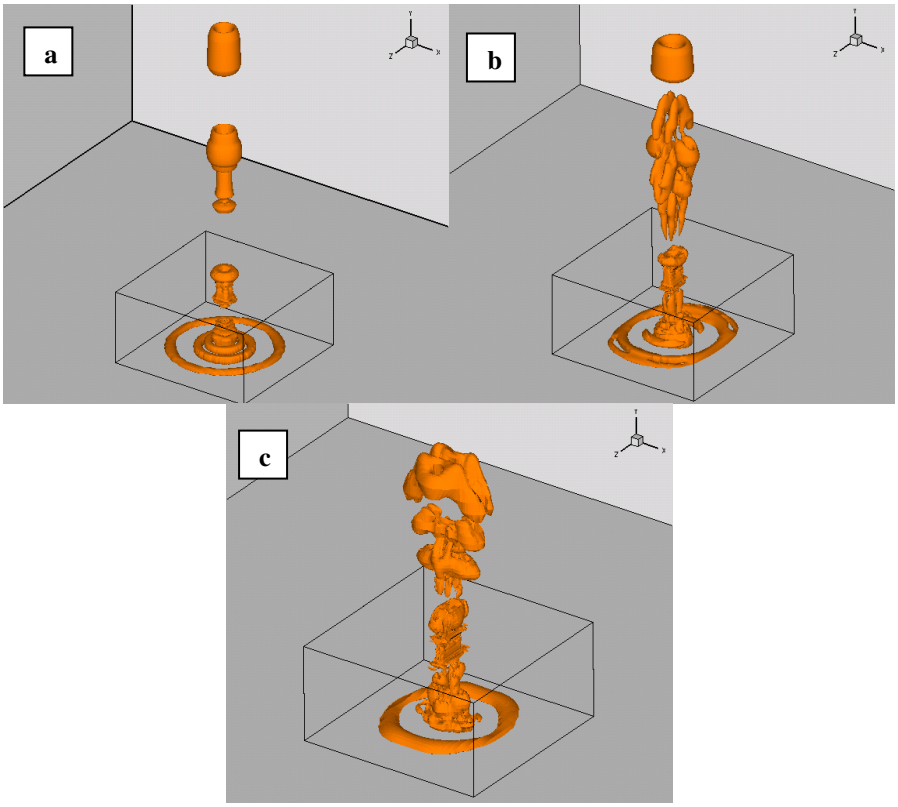

Figure 4 Iso-surfaces of eigenvalue contour, $Re_J=227$ (a) *w/d=1, S=10.8* (b) *w/d=2, S=12* (c) *w/d=4, S=15.2*

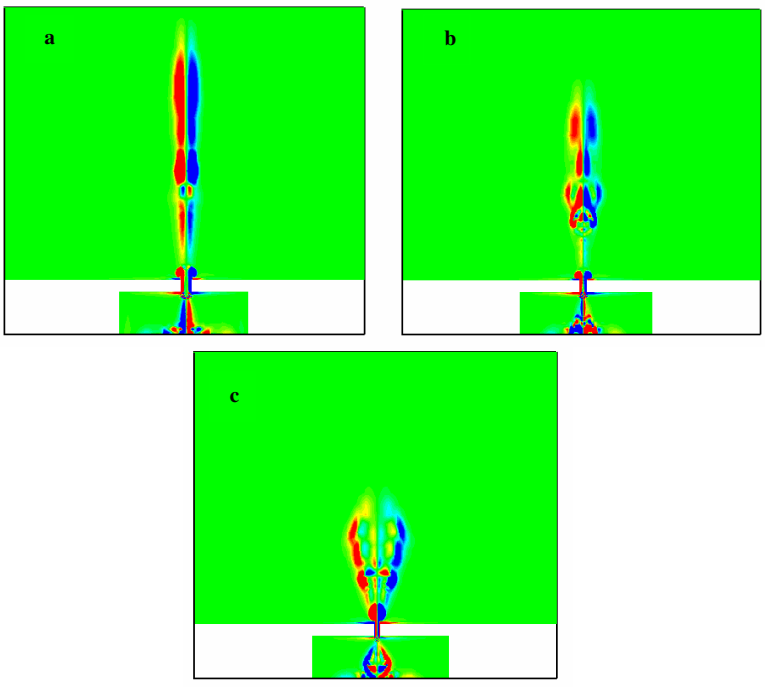

Figure 5 Vorticity contours at the slot-center in the XY-Plane (a) *w/d =1* (b) *w/d = 2* (c) *w/d = 4*

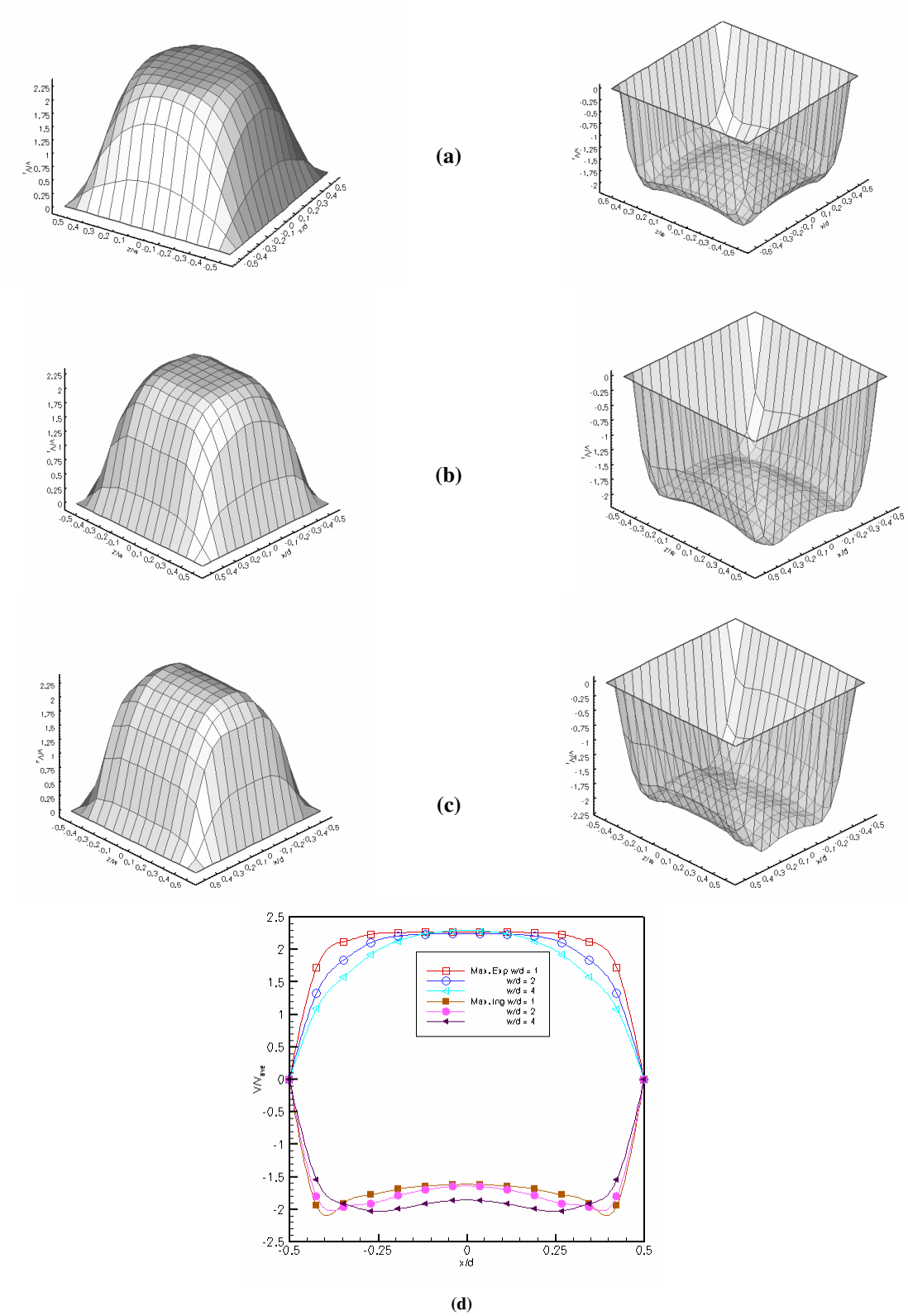

Figure (6) Normalized jet exit velocity profiles (a) *w/d=1*, (b) *w/d=2*, (c) *w/d=4*, (d) Comparison of the velocity profiles at slot center for maximum expulsion and maximum ingestion phases

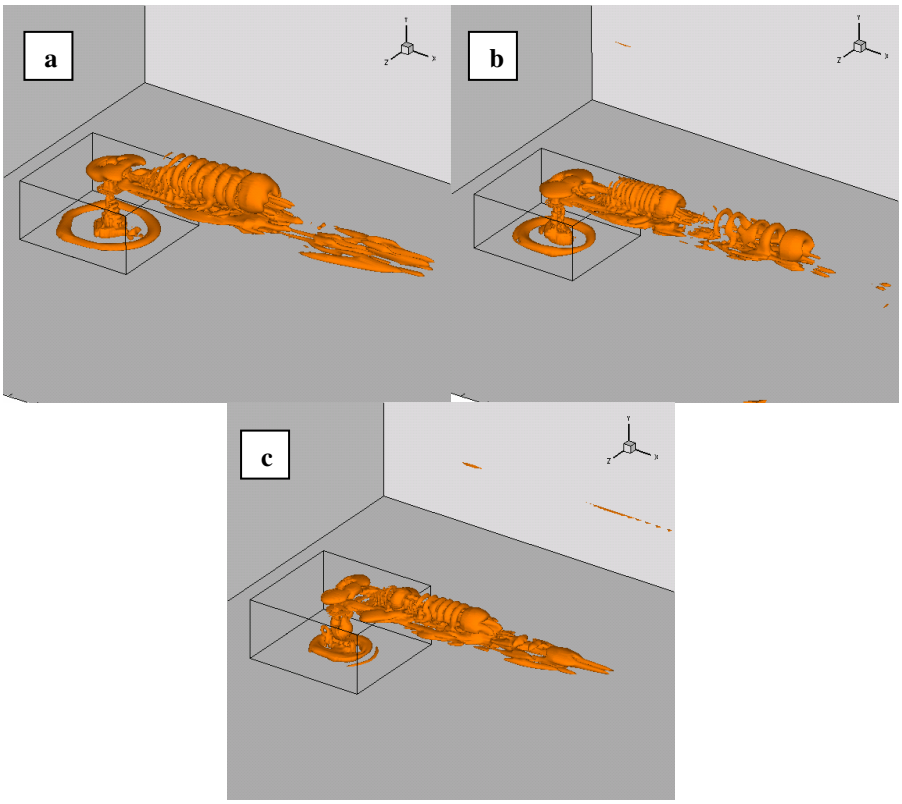

Figure 7 Isosurfaces of eigenvalue contour in the presence of external cross-flow, Re_J=227
(a) *w/d = 1* (b) *w/d = 2* (c) *w/d = 4*

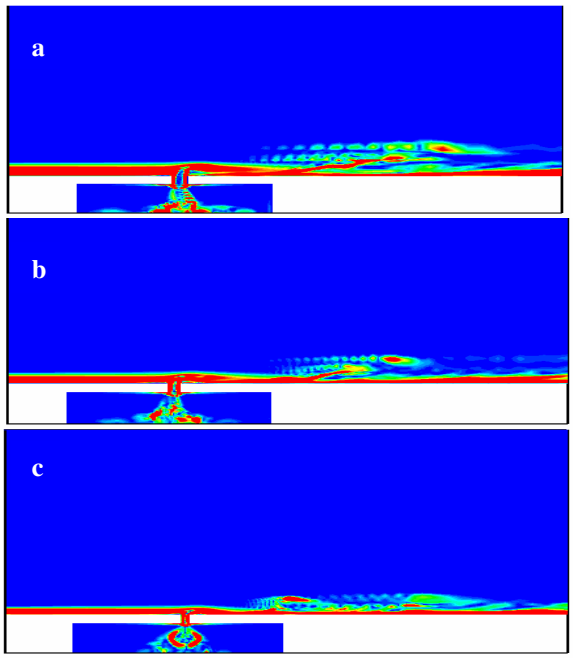

Figure 8 Vorticity contours ($\sqrt{\omega_x^2 + \omega_y^2 + \omega_z^2}$) at the slot-center in the XY-Plane
(a) *w/d =1* (b) *w/d = 2* (c) *w/d = 4*

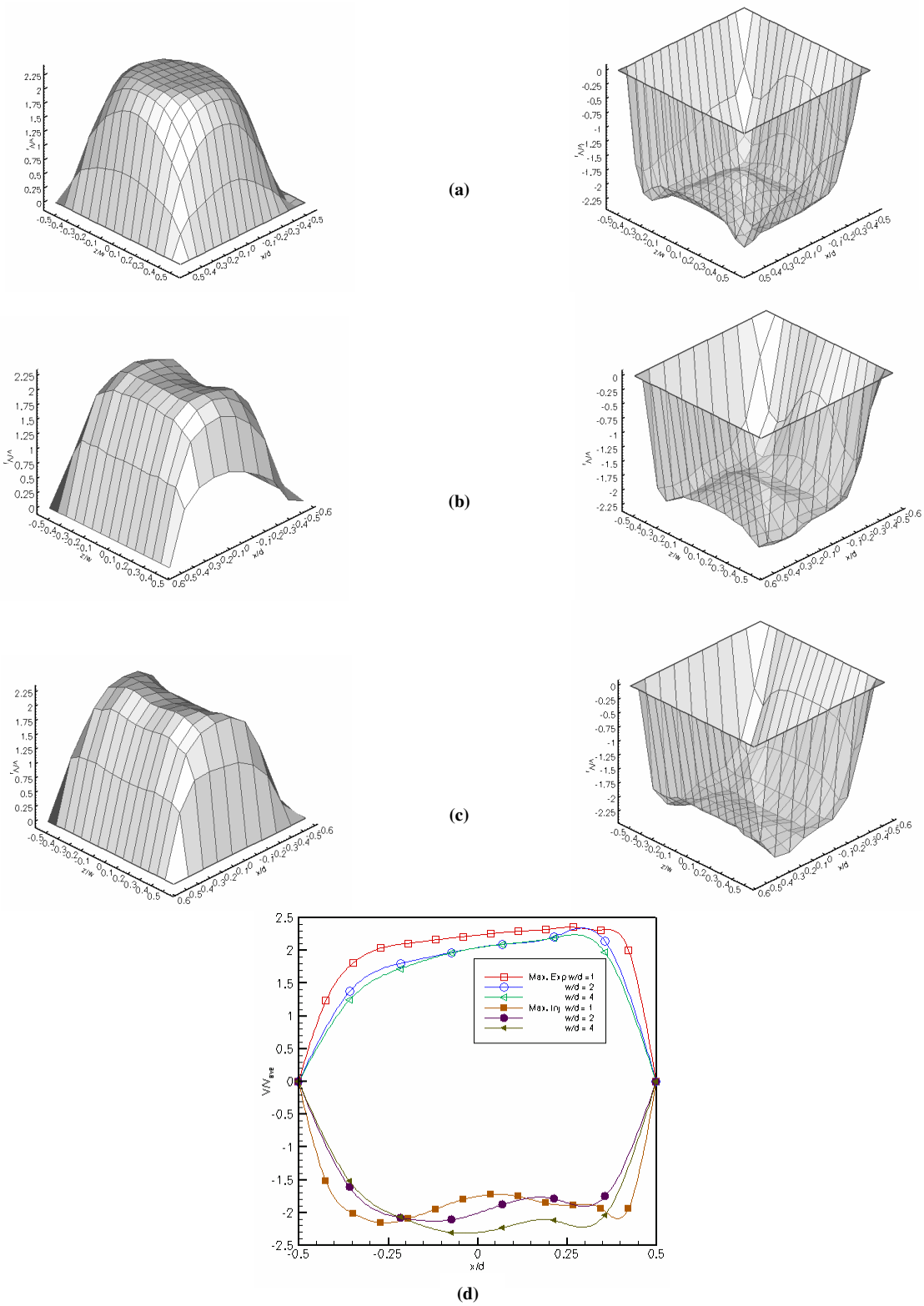

Figure 9 Normalized jet exit velocity Profiles at the slot center (a) *w/d=1*, (b) *w/d=2*, (c) *w/d=4*, (d) Comparison of the velocity Profiles for all the cases at maximum expulsion and maximum ingestion phases

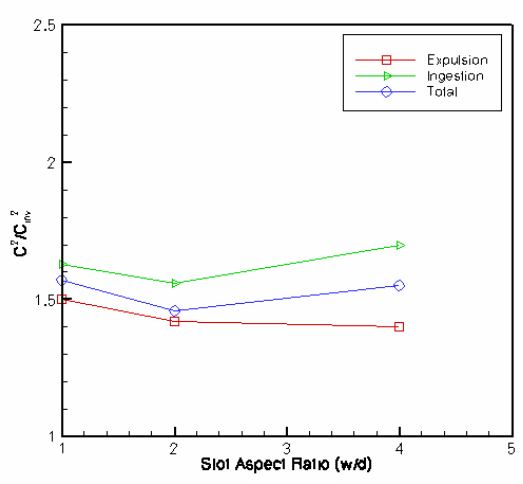

(a)

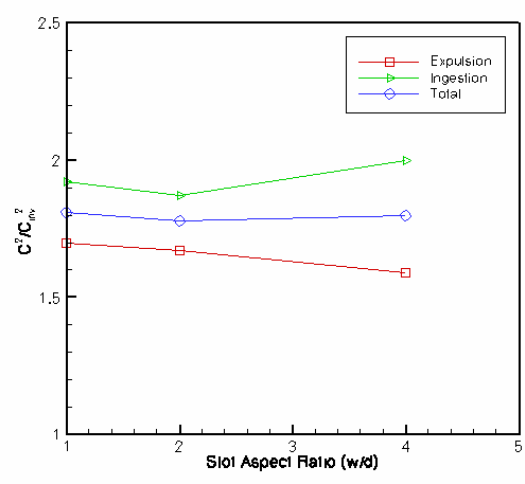

(b)

Figure 10 (a) Variation of momentum coefficient with slot aspect ratio for jet in quiescent-flow
(b) Variation of momentum coefficient with slot aspect ratio for jet in cross-flow